Journal of Materials Chemistry B

Accepted Manuscript

ROYAL SOCIETY OF CHEMISTRY

www.rsc.org/materialsB

Regeneration of Hyaline-like Cartilage and Subchondral Bone Simultaneously by Poly(L-glutamic acid) based Osteochondral Scaffold with Induced Autologous Adipose Derived Stem Cells

Kunxi Zhang [a], Shiming He [a], Shifeng Yan [a], Guifei Li [a], Danqing Zhang [a], Lei Cui [b,**], Jingbo Yin [a,*]

[a] Department of Polymer Materials, Shanghai University,

99 Shangda Road, Shanghai 200444, PR China.

[b] Medical Science & Research Center, Beijing Shijitan Hospital, Capital Medical University,

10 Tieyi Road, Beijing 100038, PR China.

[*] Corresponding author. Jingbo Yin,

99 Shangda Road, Shanghai 200444, PR China.

Tel.: +86-21-66138055, Email: jbyin@shu.edu.cn

[**] Corresponding author. Lei Cui,

10 Tieyi Road, Beijing 100038, PR China.

Tel.: +86-10-63926661, Email: cuileite@aliyun.com

Key words: cellular spheroid, adipose derived stem cells, poly(L-glutamic acid), osteochondral scaffold, inorganic-organic hybrid materials

Abstract

Osteochondral tissue engineering is challaged by the difficult regeneration of hyaline cartilage and simultaneous regeneration of subchondral bone. In the present study, /hydroxyapatite-graft-poly(L-glutamic acid) (nHA-g-PLGA) was prepared by

surface-initiated ring-opening polymerization, which was then used to fabricate osteogenic scaffold (scaffold O) instead of nHA to achieve better mechanical performance. Then, a single osteochondral scaffold was fabricated by combining poly (L-glutamic acid) (PLGA)/chitosan (CS) amide bonded hydrogel and PLGA/CS/nHA-g-PLGA polyelectrolyte complex (PEC), possessing two different regions to support both hyaline cartilage and underlying bone regeneration, respectively. Autologous adipose derived stem cells (ASCs) were seeded into the osteochondral scaffold. The chondrogenesis of ASCs in scaffold was triggered *in vitro* by TGF-β1 and IGF-1 for 7 days. *In vitro,* chondrogenic scaffold (scaffold C) exhibited the ability to drive adipose derived stem cells (ASCs) aggregate to form multicellular spheroids with diameter of 80-110 μm in-situ, thus promoting the chondrogenesis while limiting COL I deposition when compared to ASCs adhered in scaffold O. Scaffold O showed the ability of binding abundant BMP-2. Osteochondral scaffolds with induced ASC spheroids in scaffold C and bonded BMP-2 in scaffold O were transplanted into rabbit osteochondral defects as group I for *in vivo* regeneration. At the same time, osteochondral scaffolds with only bonded BMP-2 in scaffold O and bare osteochondral scaffolds were filled into rabbit osteochondral defects to serve as group II and group III, respectively. After 12 weeks post-implantation, cartilage and subchondral bone tissues were both regenerated with the support of induced ASC spheroids and bonded BMP-2 in group I. However, in group II, cartilage was not repaired while subchondral bone was regenerated. In group III, both the regeneration of cartilage and subchondral were limited.

1. Introduction

Articular osteochondral defect involves damage to both cartilage and the underlying subchondral bone, and represents a major challenge for the orthopedic community [1]. Many researches focus on cartilage regeneration for its extremely limited healing ability. Actually, subchondral bone, which plays a key role in osteoarthritis (OA) on set and progression, is of great importance to support cartilage regeneration [2]. Osteochondral tissue engineering, involving simultaneous regeneration of cartilage and bone, has been considered as an optimal model system for developing effective strategies aimed at regenerating complex tissues [3].

For cartilage layer, techniques currently used to start *in vitro* chondrogenesis of mesenchymal stem cells (MSCs) share a cell aggregation step as a prerequisite for commitment to the chondrogenic lineage, in order to duplicate "condensation" that takes place *in vivo* during limb development [4]. However, currently, most scaffolds supported MSCs adhesion and spreading, thus encouraging fibrous matrix production [5]. To mitigate the challenges associated with current cartilage tissue engineered scaffold design strategies, we have proposed to construct a porous swollen scaffold based on amide bonded poly (L-glutamic acid) (PLGA) and chitosan (CS) to weaken cellular adhesion while support in-situ birth of multicellular spheroids, in order to enhance the chondrogenesis of MSCs while limiting fibrous matrix production, further promote hyaline-like cartilage regeneration [6]. In addition, osteochondral scaffold was proposed here to accelerate mineralized bony tissues regeneration simultaneously with hyaline-like cartilage restoration, for the purpose of supporting

the homeostasis and integrity of neo-cartilage.

For subchondral bone layer, currently, considerable interest has been generated in organic-inorganic hybrid materials to mimic the bone matrix components which are collagen I and hydroxyapatite (HA). As the biomimetic bone substitute materials, collagen-calcium phosphate biocomposites have the unique capacity to bond to bone directly [7]. When combined with polymeric materials, calcium phosphates endow the scaffold with high stiffness [8]. Collagen-calcium phosphate biocomposites have produced some encouraging results [9,10], however, they typically comprised mechanical mixtures of pre-synthesized calcium phosphate particles suspended in collagenous matrix, leading to deficient mechanical properties and minimal resemblance to natural bone [7]. To mitigate the challenges associated with current biocomposites, PLGA-grafted HA composite nanoparticles (nHA-g-PLGA) were prepared by surface-initiated ring-opening polymerization to mimic combination of collagen I and nHA in bone matrix. On one hand, as a synthetic polypeptide, PLGA exhibits controllable performance and protein mimicking property [11]. On the other hand, the molecular level bonded inorganic-organic hybrid material will improve nHA dispersion as well as mechanical properties of scaffold. Then the nHA-g-PLGA, instead of nHA, was introduced into PLGA and CS polyelectrolyte complex (PEC) for constructing the underlying bone scaffold.

The two layers were combined to permeate into each other to form a secure bonding, followed by lyophilization to yield porous osteochondral scaffold with a continuous and “soft” interface between regions. However, a challenge would be

raised to exert bi-lineage functionality for regenerating both cartilage and bone in a single osteochondral scaffold. To overcome this challenge, osteochondral scaffolds with gradients in bioactive signals were created. N. Mohan designed an osteochondral scaffold with opposing gradients of chondrogenic microspheres (encapsulating TGF-β1) and osteogenic microspheres (encapsulating BMP-2) [12].

In the present study, different fabricating methods (PLGA/CS based hydrogel for cartilage layer, PLGA/CS/nHA-g-PLGA based PEC for subchondral bone layer), as well as the introduction of nHA only in subchondral bone layer [13,14] endowed the two regions of osteochondral scaffold with the distinguishing BMP-2 binding capability to result in bi-lineage regeneration within osteochondral defect. Chondrogenesis of adipose derived stem cells (ASCs) could be triggered by TGF-β1 and IGF-1 *in vitro*. While osteogenesis *in vivo* may be regulated by BMP-2 bound mainly in subchondral bone layer but cartilage layer. The cells/scaffold was transplant into rabbit articular osteochondral defect for *in vivo* tissue regeneration to confirm the advantage of the present osteochondral scaffold both on hyaline-like cartilage and subchondral bone regeneration (**Fig. 1**).

2. Experimental

2.1. Materials

Calcium hydroxide, phosphoric acid, γ-aminopropyltriethoxysilane (APS) and ammonium hydroxide ($NH_3 \cdot H_2O$, 25-28%) were purchased from Sinopharm Chemical Reagent Co., Ltd., and used without further purification. Dioxane and dichloromethane were dried by refluxing with Na

and CaH_2, respectively, and used at once. Me_3SiI (stabilized with Aluminum, >95.0%) was purchased from TCI Shanghai Development Co., Ltd., and was injected in dark place. Monomer γ-benzyl-L-glutamate *N*-carboxyanhydride (BLG-NCA) was synthesized as previously described and recrystallized sufficiently before use. Poly (L-glutamic acid) (Mv = 10×10^4) was prepared from poly (γ-benzyl-L-glutamate) (PBLG), which was synthesized by the ring opening polymerization of the N-carboxyanhydride (NCA) of gbenzyl-L-glutamate in our laboratory. Chitosan (Mv = 4×10^4) with a deacetylation degree of 95% was purchased from Jinan Haidebei Marine Bioengineering Corp. (Shandong, China). N-Hydroxysuccinimide (NHS) and by1-ethyl-3-(3-dimethylaminopropyl) carbodiimide hydrochloride (EDC) were purchased from Shanghai Medpep Co., Ltd. HBr/HAc (purchased from Sigma-Aldrich). Other reagents and chemicals were of the analytical grade and used as received.

2.2. Synthesis and characterization of HA-g-PLGA composite nanoparticles

HA nanocrystals fabrication. The HA nanocrystals were prepared through a chemical precipitation and hydrothermal technique. The reaction equation was: $6H_3PO_4 + 10Ca(OH)_2 \rightarrow Ca_{10}(PO_4)_6(OH)_2 (HA) + 18H_2O$. An aqueous solution of H_3PO_4 (0.20M, 750mL) was added to a vigorously stirred aqueous solution of $Ca(OH)_2$ (0.25M, 1000mL) at a stirring rate of 10mL/min at 50 ^oC. The pH of the suspension was adjusted to 7-8 with ammonia water after completing addition of H_3PO_4 solution. After aging for two days, the precipitation was purified by repeated washing with deionized water for three times. The rod-like HA nanoparticles were obtained by freeze-drying.

Amino-functionality of HA nanocrystals. The HA nanocrystals were prepared through a chemical precipitation and hydrothermal technique. The APS (2.210 g, 10 mmol) was added into

500 mL 10% aqueous alcohol solution. The mixture was stirred at room temperature for half an hour, followed by adding 5 g nHA. After stirring for another 3 h, the pH of the mixture was adjusted to pH 9-10 with ammonia water, after which the reaction continued for 3 h again. After washing, filtration and freeze-drying, amino-functional nHA (nHA-NH_2) was obtained and stored in vacuum drying oven.

Synthesis of HA-*g*-PLGA composite nanoparticles. nHA-NH_2 solid initiator, BLG-NCA monomer and anhydrous dioxane were added to a 100mL dry eggplant-shaped flask, and the air in the flask was extracted and replaced with water-free nitrogen for five times. The mixture was dispersed via ultrasonic treatment for 30 minutes and then stirred for 3 days at 25 °C. After precipitating in ethanol, filtration, and washing with dioxane for several times to remove the unbonded polymer, nHA-*g*-PBLG composite particles were obtained and dried under vacuum. The nHA-*g*-PLGA was synthetized via deprotection of benzyl groups in nHA-*g*-PBLG. It was accomplished by dissolving nHA-*g*-PBLG (0.5 g) in anhydrous dichloromethane (25 mL), following by addition of excess Me_3SiI (0.20 mL), and the mixture was stirred under nitrogen atmosphere in dark environment at 37 °C for 20h. The nHA-*g*-PLGA was then isolated by adding the mixture to ethyl ether (250 mL) saturated with water and ethanol. The gelatinous composites were isolated by centrifugation, washing with water (3×50 mL) and ethanol (3×25 mL), and drying under vacuum.

The XPS measurements were performed with a DLMAX-2200 ((Rigaku Corporation, Japan) to ascertain the surface composition of bare and amino-functional HA nanoparticles. The FT-IR spectra were recorded on a NICOLET 380 (Thermo Electron Co., USA) FT-IR spectrometer within the region of 4000-400 cm^{-1}. The dried samples were pressed into compact pellets with KBr.

The TGA was monitored by thermogravimetry on a Q-500 (TA Instruments, USA) from room temperature to 800 °C under nitrogen flow with a heating rate of 10 °C/min. The amount of surface-grafted polypeptide was determined as a weight loss percentage during heating.

2.3. Fabrication of biomimetic bilayered scaffolds and examination of the scaffolds properties

Fabrication of biomimetic bilayered scaffolds. nHA-g-PLGA and PLGA powder was dissolved in sodium hydroxide aqueous solution to form homogeneous solution with a pH of 7. Then, CS power was added when the nHA-g-PLGA/PLGA solution was stirred at 800 rad/min. After the powder was uniformly distributed in the solution, acetic acid was added quickly until the pH reached 4.0. Keep stirring for 8h to form homogeneous polyelectrolyte complex, in which prefabricated porogenic agent, poly (lactic acid) (PLA) microspheres with diameter of 200-400 μm was also added to create large size pores. Such mixture was defined as mixture O. The mole ratios of –COOH in PLGA and nHA-g-PLGA and $–NH_2$ of CS was 1:1. The solid content (the sum of mass fraction of nHA-g-PLGA, PLGA and CS) was 3%.

PLGA was dissolved in a low concentration of sodium hydroxide solution to form homogeneous solution. Acetic acid was then used to adjust the pH of the solution to 6, followed by adding NHS and EDC in turn to activate the γ-carboxyl of PLGA. After 8h, the solution was mixed with chitosan solution (pH = 4.5) to form a homogeneous and clear mixture, which was defined as mixture C. In this paper, the solid content was 3%. The mole ratios of γ-carboxyl group and amino group were set as 1:1 to ensure the consumption of carboxyl and amino groups.

As soon as the mixture C was going to solidify to form a hydrogel, mixture O was placing on the top of mixture C for manufacturing purpose, because mixture O was flowable. After

lyophilization at -80 °C, dissolution of PLA by dichloromethane and dialysis, a porous osteochondral scaffold (scaffold O) with two different layers was obtained. Duration of PLA dissolution was more than 72 h. Chondrogenic scaffold fabricated by amide bonded PLGA/CS was defined as scaffold C. Osteogenic scaffold fabricated by nHA-g-PLGA/PLGA/CS polyelectrolytes complex was defined as scaffold O.

Examination of the scaffolds properties. The microstructure of the porous osteochondral scaffold was observed by scanning electron microscopy (SEM) (JXA-840, JEOL, Japan). The porosities of the scaffolds was measured by the liquid displacement method [11]. Ethanol was used as the displacement liquid due to its ready penetration into the pores of the scaffolds. The gradient of nHA between layers was analyzed by SEM with energy dispersive X-ray spectroscopy (EDX).

To measure the swelling behavior of the osteochondral scaffolds, samples (scaffold C, scaffold O and scaffold OC) with dimensions of ø4×6mm were vacuum dried for 3 h. The dry weights of the scaffolds (W_d) were immediately measured. Afterwards, the scaffolds were immersed in phosphate buffered saline (PBS) solution at 37 °C and weighed at preseted time points to determine the wet weights (W_w). The swelling ratio of the scaffolds was calculated using the following formula: Swelling ratio = $(W_w-W_d)/W_d$

The storage modulus measures the stored energy, representing the elastic portion, which was given by Rheometer (AR-G2, TA Instruments Inc.) automatically, with standard steel parallel-plate geometry of 12 mm diameter. The scaffolds were subjected to a frequency sweep at a fixed shear strain (1%) and temperature (37°C), the angular frequency was increased from 1 to 100 rad s^{-1}. The scaffolds were tested in wet state. An immersion ring for a standard Peltier plate was

equipped for the immersion of the samples during the experiment in wet state.

The compressive performance of scaffolds was evaluated by an Instron-5869 mechanical tester with the cross speed of 1mm/min in ambient atmospheric conditions. The compressive modulus was given by the tester automatically. The shear modulus is concerned with the deformation of a solid when it experiences a force parallel to one of its surfaces while its opposite face experiences an opposing force. The anchorage performance of the osteochondral scaffolds was evaluated through shear modulus and tested by a push-off test on an Instron-5869 mechanical tester, with the cross speed of 1mm/min in ambient atmospheric conditions.

To analyze the charge density of scaffold C and scaffold O, the two scaffold were grinded into powder. Then the surface zeta potential was measured by an electrokinetic analyzer for solid samples (SurPASS, Anton Paar, Austria).

2.4. BMP-2 binding and release

BMP-2 binding. Both scaffolds (5 mg) were incubated with 3% (w/v) bovine serum albumin (BSA) in PBS for 2 h. Then 500 ng of BMP-2 (human recombinant BMP-2, R&D) dissolved in 3% BSA (in PBS) was added, after which the suspension was left overnight at 4 °C. After being washed by PBS for three times, the scaffolds were freeze-dried and grinded, followed by incubating with HRP-conjugated mouse monoclonal anti-human BMP-2 at room temperature for 2 h. Finally, tetramethylbenzidine (TMB, from BMP-2 Quantikine ELISA Kit) was used to detect scaffold binding BMP-2 specifically according to the manufacturer's instructions.

Quantification of BMP-2 release. The freeze-dried BMP-loaded scaffold C and scaffold O (both 5 mg) were immersed in 1000 μL of release buffer at 37 ^{o}C. Then the supernatant was

collected at 3, 7 and 14 days. The release media was replenished with an equal amount of fresh buffer. The amount of BMP-2 in the release medium was measured by the BMP-2 ELISA kit. The solution absorbance was measured at 450 nm using SpectraMax M2 (Molecular Devices, US).

2.5. Isolation and culture of rabbit ASCs

The experimental protocol was approved by the Animal Care and Experiment Committee of Shanghai Jiao Tong University School of Medicine. ASCs were isolated according to our previous work [11]. Autologous subcutaneous adipose tissue was removed from the nape of New Zealand white rabbits (8-months-old males weighting 2.5 kg-3.0 kg. The rabbits were thin, but after the harvest of adipose tissue, the rabbits were allowed to recover for 4 weeks in the laboratory animal room before the articular surgery), washed three times with 0.1 M phosphate-buffered saline (PBS, pH=7.4), then cut into small pieces, digested with 0.1% type I collagenase (Washington Biochemical Corp, USA) at 37 °C for 60 min. After centrifuging at 1200 g for 10 min, ASCs collected at the bottom of the tube were then resuspended and cultured in LG-DMEM supplemented with 10% FBS, 50 μg/mL ascorbic acid, 100 U/mL penicillin, and 100 μg/mL streptomycin in Φ 100 mm culture dishes (Falcon, USA) at 37 °C in a 5% CO_2 incubator. When reached subconfluence, cells were passaged after trysinization (0.05% trypsin and 0.02% EDTA), and ASCs prior to passage 3 were used in the following study.

2.6. Cell seeding, cellular distribution and proliferation in scaffold

The scaffold was sterilized by soaking in 75% alcohol for 2 h and washed 3 times with PBS. The excessive medium left within scaffold was removed by extensive suction. Then the scaffold was immersed in BMP-2 solution to bind BMP-2 as described in 2.4. The third-passage ASCs

were harvested by trypsinization and resuspended in culture medium at a concentration of 5×10^7 cells/mL. Cell suspensions of 50 μL were evenly dropped into scaffolds. After being incubated for 4 h, the cell-scaffold constructs placed in 24-well plate were added with 1 mL of growth medium. After 24 h of incubation, the cell-scaffold constructs were transferred into new wells for subsequent cultured *in vitro* for 1 week with chondrogenic inducing medium (the growth medium further supplemented with 10 ng/mL transforming growth factor-β1 (TGF-β1), 100 ng/mL insulin-like growth factor-1 (IGF-1), 40 ng/mL dexamethasone and 6.25 mg/Ml transferrin (all from Sigma-Aldrich)) [11].

Extracellular matrix (ECM) deposition of ASCs in osteochondral scaffold in inducing medium was observed by SEM examination at 1 week post-seeding. To visualize the growth and spatial distribution of ASCs in osteochondral scaffold, ASCs were pre-labeled with fluorescent 3,3'-dioc tadecyloxacarbocyanine perchlorate (DiO) dye (Molecular Probes, USA) at 37 ℃ for 20 min before seeding. The labeled cells were then seeded into osteochondral scaffold as described above. The cells grown on the scaffold were observed by a confocal laser microscope (FV-1000, Japan, Instrumental Analysis and Research Center, Shanghai University) at 4 h, 72 h and 1 week after seeding [11].

Cell numbers either in the scaffold C or Scaffold O at 1, 3, 5, 7, 10 and 14 days post-seeding both in growth medium and induced medium were quantified by DNA assay using Hoechst 33258 dye (Sigma-Aldrich) according to previous work [11]. Briefly, the collected cell/scaffold constructs were crushed for full lysis with proteinase K (Sigma) at 56 ^{o}C overnight. DNA content in the lysate was quantified spectrofluorometrically using Hoechst 33258 dye (Sigma).

2.7. Chondrogenic and osteogenic differentiation of ASCs in osteochondral scaffold

Cell-scaffold complexes collected at 1 week post-seeding were transferred into microcentrifuge tubes, and rinsed with doubly-distilled H_2O, lyophilized for 12 h followed by adding 1 mL cold H_2O, and incubated at 4 °C overnight. After lysis with repeated freeze thawing and sonication cycles, specimens were centrifuged for 3 min at 10,000 rpm. The precipitate was subjected to COL II and COL I assay using a Native Type II Collagen Detection Kit (Chondrex, USA) and a Native Type I Collagen Detection Kit (Chondrex, USA) according to the manufacturer's instructions, respectively. The supernatant was collected for GAG determination using 9-dimethylmethylene blue chloride solution (DMMB) (Sigma-Aldrich).

A method of quantitative PCR was carried out to further evaluate the chondrogenic and osteogenic differentiation of ASCs. Total RNA was extracted from cells [11]. The RNA concentration of the extract was determined from the optical absorbance at 260 nm. cDNA was synthesized using PrimeScript 1st Strand cDNA synthesis kit (TaKaRa). The reactions were performed and monitored in a MyCycler PCR (Bio-Rad). Real-time PCR was performed using quantitative real-time amplification system (CFX96, Bio-Rad, US). SybrGreen PCR MasterMix was used in each reaction. Relative expression levels for each gene of interest were calculated by normalizing the quantified cDNA transcript level (cycle threshold) to that of the GAPDH. Besides, the relative gene amount of non-induced group at 0 week was set as 1. Gene expression of collagen type II (COL II), collagen type I (COL I), aggrecan, SOX9, ALP and OCN was evaluated at 1 week post-seeding. Primer sequences were placed in Table 1.

2.8. Implantation of engineered cartilage constructs

Osteochondral scaffolds were fixed with 2 mm scaffold C and 4 mm scaffold O. Autologous ASC-scaffold constructs after being chondrogenic induced *in vitro* for 7 days were implanted to repair articular osteochondral defects. A defect of 4 mm in diameter and 6 mm in depth was created by drilling at non-weight bearing area of femur trochlea on the femoropatellar groove of the knee joints using a trephine. A total of 2 defects were created in one rabbit. Accordingly [3], no-treatment defect showed limited healing ability. Thus no-treatment control group was not performed in the present study. Three groups were carried out to evaluate the *in vivo* osteochondral tissue regeneration. Groups were list in Table 2. Twenty one rabbits aged 8 months were used to carry 42 samples for each time point. The total number of rabbits was 42. Animals were euthanized respectively at 6 weeks and 12 weeks post-surgery for sample harvest.

2.9. Evaluation of osteochondral tissue regeneration in vivo

For each time point of each group, there were 7 animals with 14 samples. 7 samples from 7 animals were used to do the histological examination. However, due to the samples lose in processing, not all the 7 samples were involved in histological examination. The histological study design was presented in Table 3. Of note, for group I, 1/2 area of 7 samples at 12 weeks were divided before fixed in neutral buffered formalin to do EDX analysis. The other 7 samples from the 7 animals in group I at each time point were used to do the biomechanical and biochemical analysis. But due to the samples lose in processing, 5 samples at each time point were involved in biomechanical and biochemical analysis.

Histological examination, Immunohistochemical staining. The engineered tissues (6 weeks and 12 weeks) used to do the histological test were fixed in neutral buffered formalin, decalcified

in formic acid, embedded in paraffin, sectioned (5 μm thick) and then deparaffinized with xylene followed by hydration in ethanol solutions of decreasing concentrations (100% to 70%) [11]. Histology of tissue was observed by hematoxylin and eosin (H&E) staining, safranin O & fast green staining. Expression of COL I and COL II in the engineered tissue was examined by immunohistochemical staining. The histological results were scored blindly according to Holland TA with an evaluation of subchondral bone regeneration [15]. The grading was performed by 5 samples from 5 rabbits in group I at 6 weeks, 5 samples from 5 rabbits in group I at 12 weeks, 7 samples from 7 rabbits in group II at 6 weeks, and by 6 samples from 6 rabbits in group III at 12 weeks, 5 samples from 5 rabbits in group III at 6 weeks, 5 samples from 5 rabbits in group III at 12 weeks. 4 sections were chose from 1 sample. Thus, totally 20 sections from group I at 6 weeks, 20 sections from group I at 12 weeks, 28 sections from group II at 6 weeks, 24 sections from group II at 12 weeks, 20 sections from group III at 6 weeks, and 20 sections from group III at 12 weeks were involved in grading. The grading was performed by 3 individuals (including Kunxi Zhang, Shifeng Yan and Danqing Zhang) in a blind test fashion. Another three persons except Kunxi Zhang, Shifeng Yan and Danqing Zhang will carry out the grading when there was significant score discrepancies, which was not happen in the present study. Histological grading is presented in Table 4.

Biomechanical analysis of the engineered cartilage. Samples at 6 and 12 w in group I used for the biomechanical and biochemical analyses were trimmed along the rim of the regenerated tissues by a trephine. The normal samples were also harvested by the same method. The harvest parts (semi-circle with 2 mm in diameter) were tested in a material testing machine (Zwicki-line Z 2.5KN) at a speed of 1 mm min^{-1}. The ratio of stress to strain was defined as the compressive

modulus.

Biochemical analysis of the engineered cartilage. The other harvest parts (the other semi-circle with 2 mm in diameter) at 6 and 12 w in group I used for biochemical analysis were collected, weighted (average weight 7.1 ± 2.8 mg for group I at 6 weeks, average weight 4.6 ± 1.7 mg for group I at 12 weeks, average weight 5.4 ± 2.2 mg for native tissue) and crushed. Then, their GAG and COL II contents were analyzed in a similar manner as described in the previous section.

EDX analysis of the engineered cartilage. Samples collected were freeze-dried and analyzed by SEM with energy dispersive X-ray spectroscopy (EDX).

2.10. Statistical analysis

For experiments of scaffold physical and chemical properties, each measurement was based on duplicate analysis of at five independent experiments (N=5). For in vitro experiments, ASCs from five individual rabbits were subjected, and each measurement reported was based on duplicate analysis of at three independent experiments. For in vivo biochemical analysis and biomechanical analysis, five samples at 6 w and five samples at 12 w from group I were subjected. Data was all reported as mean ± standard deviation (SD). One-way analysis of variance (ANOVA) was performed to reveal statistical differences. 4 repeated measures ANOVA was performed for the grading of the histological examination to reveal statistical differences. A p-value of less than 0.05 was considered statistically significant.

3. Results

3.1 Synthesis of nHA-g-PLGA composite nanoparticles

The nHA-g-PLGA was synthesized by initiating NCA polymerization on the surface of nHA-NH_2 particle which was amino-functionalized from nHA, followed by removing the benzyl-protecting groups with Me_3SiI (**Fig. 2a**). As shown in **Fig. 2b**, the TEM micrograph showed that the nHA was rod-like crystals with the mean size of 120-130 nm in length and 20-30 nm in width. Of noticed, nHA tended to aggregate into microscale clusters but exhibit improved dispersion ability after grafting PLGA.

The XPS technique was applied to confirm the grafted PLGA on the surface of nHA. Characteristic peaks at binding energy of 532.8 eV, 401.8 eV, 346.6 eV and 133.0eV are attributed to O1s, N1s, Ca2p, and P2p, respectively. Presence of the nitrogen (N), decrease of calcium (Ca) & phosphorus (P) peaks in **Fig. 2c**, and presence of amide bond (288.2 eV), carboxyl group (289.0 eV), amino group (286.0 eV) in **Fig. 2d** illustrated that nHA was covered by PLGA. Moreover, FT-IR spectra of nHA-*g*-PLGA exhibited not only the characteristic peak of PO_4^{3-} at 1040cm^{-1}, but also the characteristic peaks of α-helix amide I at 1652cm^{-1}, amide II at 1546cm^{-1} and carboxylic acid side chains at 1722cm^{-1}, confirming the successful polymerization (**Fig. 2e**).

To accurately determine content of shell and core parts, the grafting rate (Gr) was defined as follows: Gr = (mass of grafted polypeptide)/(mass of entire particle). A direct assay of the Gr of nHA-g-PLGA was provided by TGA (**Fig. 2f**), the Gr of nHA-g-PLGA was measured through the change of percent weight loss between 200 and 800°C, where the weight loss belongs to the polymer material. This calculated method was superior to some others referring to a fixed sample, because it contributes

to eliminate individual differences and samples of various polypeptide contents contain different moisture or solvents. The weight loss results were shown in **Fig. 2g**. With added monomer concentration ([M]) increasing, the percentage of combustible polymer material increased. Moreover, the estimated Gr of nHA-g-PLGA was obtained based on hypothesis that no polypeptide chains fracture and no nHA-polypeptide conjugation rupture happened and the deprotection was complete. Results revealed that Grs of nHA-g-PLGA were extremely close to estimated results, showing the difference less than 3.42%. It can be concluded that the Me_3SiI was an ideal debenzylation reagent for the present composite materials. Accordingly, the Gr could reach as high as 50%.

3.2 Preparation of osteogenic scaffold (scaffold O)

The improved colloidal stability of nHA in solution is of great importance for preparation of polymer-inorganic composites. As illustrated in **Fig. 3a**, nHA precipitated within several minutes. While nHA-g-PLGA could disperse uniformly. The colloidal stability increased with the improvement of Gr. The improved dispersion and colloidal stability indicated strong interfacial interaction when involved in scaffold construction. Thus, nHA-g-PLGA with Gr of 50% was introduced into the PLGA/CS polyelectrolytes complex through electrostatic interaction to fabricate the subchondral scaffold. At the same time, nHA was introduced into PLGA/CS polyelectrolytes complex through mechanical blending as the control group. After freeze-drying at -20 ^{o}C, two porous scaffolds were formed with similar pore size of 150-200 μm as shown in **Fig. 3b,c**. Magnification images

(**Fig. 3d,e**) showed that micro-clusters spread uniformly on the walls in nHA-g-PLGA/PLGA/CS scaffold, which were confirmed to be nHA by SEM-EDS (**Fig. 3f,g**). But on the walls of PLGA/CS scaffold contained mechanical blended nHA, it was found that nHA aggregated, resulting in a non-uniformed distribution (**Fig. 3h,i**).

Such different distribution of nHA will lead to different mechanical properties. As shown in **Fig. 3j**, under the same nHA-polymer ratio, storage modulus of nHA-g-PLGA/PLGA/CS scaffold was significant higher than that of nHA/PLGA/CS scaffold. Especially when nHA-polymer ratio was 2:10, the storage modulus of nHA-g-PLGA/PLGA/CS scaffold was 4.7 fold of that performed by nHA/PLGA/CS scaffold. Besides, presence of nHA-g-PLGA could improve the storage modulus of PLGA/CS polyelectrolytes scaffold as high as 10900±601 Pa. But further increasing the nHA-polymer ratio to 3:10 led to the decrease of storage modulus to 5100±489 Pa.

3.3 Preparation of chondrogenic scaffold (scaffold C)

At the same time, N-Hydroxysuccinimide (NHS) and 1-ethyl-3-(3-dimethylaminopropyl) carbodiimide hydrochloride (EDC) were employed to activate the γ-carboxyl groups of PLGA, followed by reacting with the amino groups of CS to yield a homogeneous hydrogel (**Fig. 4a**). The gelation time, which had a great relationship with the combination of scaffold C and scaffold O, was evaluated by dynamic mechanical test on a torque rheometer. As shown in **Fig. 4b**,

when the storage modulus was equal to the loss modulus at 57.3 s, the solidification of PLGA/CS solution happened. Thus, in order to evaluate the optimize time point to construct the osteochondral scaffold with the highest shear strength, 50, 60 and 70 s were chose to carry out the combination of the two scaffolds. The result indicated that the shear strength decreased from 0.15±0.02 MPa to 0.07±0.01 MPa along with the increase of combination time (**Fig. 4c**).

3.4 Preparation of osteochondral scaffold (scaffold OC)

To get the best combination of the two layers, 50 s was thus chose to be the combination time point to place nHA-g-PLGA/PLGA/CS polyelectrolytes complex on the top of PLGA/CS gel. PLA microspheres with diameter of 200-400 μm were mixed into nHA-g-PLGA/PLGA/CS polyelectrolytes complex to form pores with large size to accommodate bone regeneration. After lyophilization and dissolution of PLA, a porous scaffold OC was achieved with two different layers, which were illustrated by macrographic observation and SEM. In addition, EDX analysis showed distinctly different Ca, P content of scaffold C (low Ca, P content) and scaffold O (high Ca, P content) (**Fig. 5a**). **Fig. 5b-e** showed the scaffold C with pore size of 180-300 μm possessed smooth pore surfaces. While scaffold O exhibited rough pore surfaces and a pore size of 200-400 μm. At the same time, smaller pores less than 100 μm formed through freeze-drying process at -80 ^{o}C. And the porosity of the single scaffold C, scaffold O and the whole osteochondral scaffold were all more than 90%.

The swelling ratio of scaffold C, scaffold O and scaffold OC were investigated in

PBS at physiological pH (7.4) and temperature (37 ^{o}C). It was found that the swelling ratio of the scaffold OC reached a maximum value of approximately 15.48±0.56% (mass%) after 4h, which was higher than that of scaffold O but lower than that of scaffold C (**Fig. 5f**). Compressive modulus of wet scaffold OC was 9.42±1.03 KPa (**Fig. 5g**). The interfacial sheer strength for the scaffold OC was 0.123±0.021 MPa as shown in **Fig. 5h**. Failures occurred at the osteochondral interface while displacement between chondrogenic layer and osteogenic layer reached at 3.5 mm.

During the initial design, scaffold C was expected to carry few charges to bind limited BMP-2, while scaffold O should possess abundant charges to bind more BMP-2. Thus, the zeta potential of the two scaffolds was quantified. As revealed in **Fig. 5i**, scaffold O exhibited a zeta potential as high as 2.4 fold of that of scaffold C. Being consistent with zeta potential, BMP-2 association in scaffold C was 12.2±4.2 ng/mg scaffold, but in scaffold O, BMP-2 was bound as high as 80.6±6.8 ng/mg scaffold (**Fig. 5j**). *In vitro* BMP-2 release from scaffolds was evaluated by incubating BMP-2 loaded scaffolds in the release buffer for up to 14 days. As shown in **Fig. 5k**, after 3 day, the cumulative release of 48.7% and 42.7% were achieved in scaffold C and scaffold O, and kept increasing to 57.1% and 51.3% after 7 days, corresponding to 5.2±1.1 ng/mg scaffold and 39.2±1.7 ng/mg scaffold residual BMP-2 in scaffold C and scaffold O for *in vivo* release, respectively.

3.5 ASCs attachment, distribution and growth in scaffold OC

ASCs suspension (5×10^7 cells/mL) was pipetted into the scaffold OC. Through

confocal laser scanning microscopy (**Fig. 6a,b**), Dio pre-labeled ASCs were observed to distribute evenly within scaffold C at 4 h post-seeding, and exhibited a rounded profile which aggregated spontaneously to form cellular spheroids within most pores of scaffold at 72 h. However, in scaffold O, labeled ASCs were dispersed along the scaffold walls at 4 h, further becoming more intensive at 72 h post-seeding (**Fig. 6c,d**). And finally, an osteochondral scaffold showed different cellular distribution inside, and ASCs dispersed in scaffold O did not spread into scaffold C (**Fig. 6e**). SEM image in **Fig. 6f** exhibited the cellular spheroids with a diameter of 80-110 μm, and individual cells in spheroid could no longer be distinguishable. But in scaffold O, SEM image confirmed that ASCs did adhere to the scaffold, and produced matrix to cover the walls of the pores (**Fig. 6g**). DNA quantitative assay showed that cell numbers in scaffold C cultured in either growth or chondrogenic medium did not change significantly during the whole *in vitro* culture (N=5, $P<0.05$) (**Fig. 6h**). However, in scaffold O, ASCs numbers increased dramatically with time in either growth or chondrogenic medium (**Fig. 6i**).

3.6 Differentiation of ASCs in scaffold OC

The *in vitro* induction of ASCs/scaffold OC was last for 7 days to trigger the chondrogenic differentiation by a combination of TGF-β1 and IGF-1 before implanting *in vivo*. To determine the chondrogenesis of ASCs, the content of cartilage specific ECM, including GAGs and COL II, was quantified. The amount of GAGs in scaffold C and scaffold O increased to 0.24±0.03 μg/μg DNA and 0.16±0.02 μg/μg DNA, respectively. The amount of COL II in scaffold C and scaffold O reached

2.47±0.32 ng/μg DNA and 1.38±0.41 ng/μg DNA, respectively. Deposition of GAGs and COL II in scaffold C was higher than that in scaffold O (N=5, P<0.05). Corresponding to ECM quantitation results, the chondrogenic markers SOX9, aggrecan and COL II were expressed both in scaffold C and scaffold O during *in vitro* induction for 7 days. But these chondrogenic markers expression in scaffold C was much higher than those in scaffold O (N=5, P<0.05), indicating that the chondrogenesis of ASCs was enhanced in spheroids. Of noticed, COL I deposition and COL I gene expression were lowly detectable, especially in scaffold C. The relative levels of gene expression in the non-induced group at 0 week was set as 1 (**Fig. 6j,k**).

3.7 General observation, histological and immunohistochemical staining of repaired tissues

As the table 2 shown, group I was treated with induced ASC spheroids in scaffold with BMP-2; group II was treated with bare scaffold with BMP-2; group III was treated with bare scaffold. All rabbits moved freely and appeared to be healthy throughout the whole post-implantation period. Macrographic observation showed that in group I, defects that filled with chondrogenic induced ASC spheroids and scaffolds binding BMP-2 were repaired with newly formed whitish engineered tissue at 6 weeks post-implantation. After further matured at 12 weeks, the neo-tissue exhibited a similarity in color and texture to the native cartilage. In group II, defects that filled with scaffolds binding BMP-2 were occupied partly by whitish and tenacious cartilage-like tissues at 6 weeks post-implantation, which collapsed after 12

weeks. In group III, defects filled with bare scaffolds showed newly formed whitish and soft tissue at 6 weeks post-implantation, texture of which was clearly different from native cartilage. And after 12 weeks, the tissues were collapsed and no repair was found (**Fig. 7**).

Hematoxylin and eosin (H&E) staining further confirmed the above general observations. No evidence of a persistent inflammatory response was observed in all groups at 6 and 12 weeks. In group I, newly generated engineered tissue at 6 weeks had fully filled the defects (**Fig. 7a**). Neo-tissue in chondral region was uneven and thicker than the surrounding normal cartilage, showing high cell density and disordered cellular arrangement. But cartilage lacuna structure was significant. Neo-tissue in chondral region displayed continuity with underlying subchondral tissue. Trabecular bone was already presented obviously but incompletely filling, possessing similar morphology properties but higher density compared with healthy bone. When it came to 12 weeks, the new joint surface exhibited even thickness and well-integration with the native cartilage. Cells populated the defect area and were reduced in number compared with those at 6 weeks post-implantation, showing arranged in a zonal organization resembling the healthy articular cartilage. At the same time, mature trabecular bone ingrowth within subchondral region was completely integrated with the adjacent bone without visible demarcation. The tidemark could also be observed (**Fig. 7b**).

In group II, a thin and irregular layer of tissue generated in chondral region, showing unobvious cartilage lacuna structure and poor integration with underlying

tissue at 6 weeks. Also, a small amount of newly formed bone with continuous structure was observed in subchondral region, as well as un-degradable scaffolds. The neo-bone tissue did not well integrate into the adjacent host bone (**Fig. 7c**). After 12 weeks post-implantation, neo-tissue in chondral region at 6 weeks degraded and was replaced by fibrous tissue. What is more, a kind of newly formed bone-like tissue was found to invade into chondral region as shown in **Fig. 7d**. Compared with neo-tissue in subchondral region at 6 weeks, the degree of bone regeneration increased at 12 weeks. Thinner trabecular bone could be observed significantly but incompletely. Integration with native bone tissue was improved.

In group III, after surgery for 6 weeks, there were some fibroblast-like cells with elongated nuclei in chondral region. Fibrous tissues mixed with irregular and small bony islands were found in subchondral region. Scaffolds were not completely degraded (**Fig. 7e**). After 12 weeks, significant fibrous tissue was found in chondral region. Restoration of subchondral bone was also extremely poor. Quite few bone-like tissue could be observed, leaving denuded of the subchondral phase. In addition, the native subchondral bone had collapsed (**Fig. 7f**). Accordingly, the repair of osteochondral defect without any treatment was limited [3]. The present results indicated that defects treated with bare scaffold showed no significant positive effect on promoting osteochondral tissue regeneration.

Safranin O & fast green, COL II/I immunohistochemical staining were carried out to testify the deposition of GAGs, COL II and COL I, respectively. As shown in **Fig. 8**, for cartilage region, a robust expression of GAGs and COL II was found in group I,

while COL I expression was limited either at 6 weeks or at 12 weeks post-implantiation. In group II, the chondral layer exhibited slight staining for GAGs and COL II, but stronger and more extensive signal of COL I at 6 weeks. After 12 weeks post-implantiation, no deposition of GAGs and COL II could be detected. Instead, intense staining of COL I indicated that neo-tissue at 6 weeks in cartilage portion was fibrosis. In group III, weak deposition of GAGs and COL II in cartilage portion at 6 weeks was observed to be totally replaced by COL I, which was intensely stained with COL I immunohistochemistry at 12 weeks.

For subchondral bone region, as shown by staining of ECM and COL I, regenerated bone was observed at 6 weeks, and matured at 12 weeks with intense expression of COL I in group I. While in group II, the degree of bone regeneration increased slowly from 6 weeks to 12 weeks post-implantation. Thinner and insufficient trabecular bone restoration was found at 12 weeks comparing to group I and normal bone. But the regenerated bone exhibited positive effect on protecting surrounding native bone form damage. In group III, however, a small amount of trabecular bone was observed until the 12th week at the defect compartment, resulting in the collapse of surrounding native bone.

Specially, the worst repaired defects in group I, II and III at 12 weeks were presented in **Fig. 9a**. The histological grading scores (except the percent filling with neo-formed tissue) obtained for group I were better than the corresponding ones for group II and III (Table 4). In group I, the scores for the engineered cartilage 12 weeks post-implantation were better than the corresponding ones at 6 weeks.

Meanwhile, quantitative analysis of GAGs, COL II in engineered cartilages and normal cartilage further confirmed the staining results. As shown in **Fig. 9b,c**, in group I, GAGs and COL II content of neo-tissue at 6 weeks reached 83% and 68% of that of the normal osteochondral tissue, respectively; and increased to 91% and 81% at 12 weeks, respectively. The compressive modulus of the engineered tissue 6 weeks post-repair reached about 44% of that of native tissue, further increased to nearly 78% at 12 weeks (**Fig. 9d**). What is more, EDX was carried out to evaluate the Ca and P distribution across the cartilage-bone interface of undecalcified samples (**Fig. 9e**). The interesting area was from cartilage layer to underlying bone. The results showed that both Ca and P contents in engineered tissue in group I increased with the detection went from cartilage region to underlying bone region, similar to normal osteochondral tissue.

4. Discussion

Osteoarthritis is the most common degenerative joint disorder, which is the leading cause of physical disability [16]. Articular cartilage degeneration is the primary concern in osteoarthritis. Thus, articular cartilage regeneration plays a pivotal role in treating osteoarthritis [17]. At the same time, the subchondral bone is also involved in osteoarthritis. According to G. Zhen et al, subchondral bone with inhibition of TGF-β activity could lead to less degeneration of articular cartilage, thus attenuate the osteoarthritis [16]. Subchondral bone provides the mechanical support for overlying articular cartilage during the movement of load-bearing joints and undergoes constant adaptation in response to changes in the mechanical environment through modeling or

remodeling [18]. The homeostasis and integrity of articular cartilage rely on its biochemical and biomechanical interplay with subchondral bone [19]. Thus, osteochondral tissue engineering, which means simultaneous regeneration of cartilage and bone, should be taken into account.

Scaffolds serve a critical role in tissue engineering by providing an environment for cells. Basically, an ideal scaffold should be structural and functional biomimetic of the native ECM, on the purpose of promoting cellular differentiation *in vitro* and tissue regeneration *in vivo* [20]. In this respect, solutions for osteochondral tissue regeneration, which is multiple tissue regeneration, are to segregate scaffold formulations into two or more layers, with discrete changes in physical or chemical properties, but a continuous, gradual, or "soft" interface between regions that could mimic natural complex tissue structure. Lots of researches fabricated various osteochondral scaffolds for potential osteochondral tissue regeneration, such as TruFit plug. As the cell-free implant, the TruFit plug consists of two layers and is a composite of polylactide-co-glycolide, calcium sulphate and polyglycolide fibres, which was proved to show the poor characteristics of the repair tissue [21,22]. Polylactide-co-glycolide and polyglycolide fibres were proved to lead to in vivo inflammatory foreign body reactions [23]. In addition, it lacks the effective tissue induction without the pre-induced seeded cells. Thus in the present study, poly(L-glutamic acid) and chitosan was chose as the component of osteochondral scaffold for their biodegradable property with no antigenicity or immunogenicity [24]. Our previous work illustrate that the PLGA/CS scaffold could be degraded within 12

weeks [11,25]. Beside, ASCs were employed here as the seeded cell to promote the osteochondral tissue regeneration.

PLGA/CS hydrogel was designed as the cartilage layer to enhance hyaline-like cartilage regeneration. Currently in stem cell based cartilage regeneration, most of the neo-generated cartilage exhibited fibrocartilage features, which is associated with the current scaffold strategy that encourage cellular adhesion and spreading [5,26]. Instead, the dense mass of aggregated MSCs created an environment with strong cell-cell interactions that could promote the immediate differentiation of MSCs into chondroblasts, and displayed enhanced chondrogenic differentiation capacities upon induction [27]. Thus a scaffold design strategy that weaken cell-scaffold adhesion while support cellular aggregates formation was proposed to enhance MSCs chondrogenesis. In this work, after lyophilization of PLGA/CS hydrogel, a porous scaffold would be achieved, possessing high swelling behavior which contributed to the prevention of cell-scaffold adhesion and spontaneous formation of multicellular spheroids with diameter of 80-110 μm. On one hand, as the results illustrated, compared to traditional scaffold that encourage cellular adhesion, the PLGA/CS hydrogel scaffold did promote hyaline cartilage regeneration with the limitation of fibrous matrix deposition. On the other hand, compared to currently practiced cellular aggregates fabrication techniques, such as hand drop technique [28], centrifugation [29] and continuous agitation of suspension culture [30], which would cost more than two steps to be applied in cartilage tissue engineering, PLGA/CS hydrogel scaffold was more convenient, direct and effective during *in vitro* culture and *in vivo* implantation.

PLGA and CS could also be composed to mimic the natural ECM of subchondral bone. However, for complete simulation of bone ECM, in which hydroxyapatite nanocrystallites (nHA) and collagen fibrils are well organized in a hierarchical architecture over several length scales, nHA was introduced into PLGA and CS complex. nHA have been widely used as the bone substitute materials for its biocompatibility and osteoconductive properties [8-10]. The biomimesis-inspired approaches currently used to obtain inorganic-organic composite materials are based on mechanical mixing [31], co-precipitation [32] and an alternate soaking process [33]. However, a common disadvantage of all these methods is that inorganic particles cannot be distributed within the organic matrices at the nano-level. This has led to poor mechanical properties and limited applications [34]. In this paper, PLGA was grafted on nHA surface through surface-initiated NCA polymerization method following "grafting from" approach, which is more efficient to achieve high grafting density than "grafting to" approach. The results revealed that Gr of HA-g-PLGA increased as the growth of monomer concentration, and reached as high as 50%. The colloidal stability increased with the increase of Gr. PLGA grafted nHA endowed nHA with strong interfacial adhesion in PLGA/CS complex, including the electrostatic interaction between carboxyl groups of nHA-g-PLGA and amino groups of CS. The strong interfacial adhesion strengthened the mechanical properties of the scaffold compared to scaffold fabricated by dispersing nHA into PLGA/CS complex.

Besides, nHA is well known for its binding capability to deliver molecules, such as BMP-2, to bones [14,35]. The present design strategy was to carry BMP-2 in scaffold O

to accelerate subchondral bone regeneration. The *in vitro* binding of BMP-2 result exhibited a binding amount of 80.6±6.8 ng/mg scaffold in scaffold O, as high as 6.6 fold of that of scaffold C. Accordingly, -OH, $-NH_2$, and $-COO^-$ were found for BMP-2 to interact with nHA surface [14]. For $-COO^-$, the adsorption phenomenon is driven by the electrostatic interaction formed between the negative charged carboxylate groups and the Ca1 cations on the hydroxyapatite surface. While for NH_2/NH_3^+, the interaction is through the intermolecular H-bonds between the N-containing groups and the phosphate on the hydroxyapatite surface. Besides, the water-bridged H-bond is the main force for groups without net charges [14,35]. However, under the physiological conditions, proteins do not have a particular affinity to nHA due to its lack of a sufficiently high specific activity and competition from the other ions, organic molecules, and proteins [36]. Thus, in addition to nHA, PLGA and CS also took the responsibility to carry BMP-2. As two polyelectrolytes, PLGA and CS possessed plenty of carboxyl groups, amino groups and hydroxyl groups to bind BMP-2 through Coulomb force. But because of the high activation efficiency of EDC and NHS, amide bonded PLGA/CS possessed few free carboxyl groups and amino groups (**Fig. 5i**). To leave more free carboxyl groups and amino groups to bind abundant BMP-2 for *in vitro* and *in vivo* release, PLGA was conjugated with CS through electrostatic interaction. BMP-2 in both layers of osteochondral scaffold exhibited a similar burst release at 1 day *in vitro*. And after 7 days culture, there were 5.2±1.1 ng/mg scaffold and 39.2±1.7 ng/mg scaffold BMP-2 left in scaffold C and scaffold O for *in vivo* release, respectively.

Moreover, ASCs could adhere on the walls of pores of scaffold O, which was believed to associate with introduction of nHA-g-PLGA. nHA-g-PLGA could be strongly bound to PLGA/CS complex through electrostatic interaction, thus forming lots of physical cross-linking units to limit the swelling ratio of scaffold O. Results showed that swelling ratio of scaffold O was 9.24±0.49%, significantly lower than that of scaffold C (18.23±1.34%). According to A. Wörz [37], significantly swollen charged networks consisting of polyelectrolytes did not adsorb any proteins, and the cellular adhesion was inversed to the swelling ratio. In the present study, we believed that it was the limited swelling behavior of scaffold O contributed to ASCs-scaffold adhesion.

In this study, *in vitro* initiation of chondrogenesis and *in vivo* BMP-2 release were both important for successful regeneration of osteochondral tissue. The present induction strategy *in vitro* was to trigger ASCs chondrogenic differentiation for 7 days. Then the cartilage progenitor cells were transplanted with scaffold into osteochondral defects to generate both cartilage and subchondral bone. After the 7 days chondrogenic induction, ASCs either in scaffold C or in scaffold O expressed chondrogenic genes, including SOX9, aggrecan and COL II. Meanwhile, cartilage specific ECM, GAGs and COL II were found to deposit significantly. ASCs in spheroids in scaffold C showed obviously higher chondrogenic genes expression and cartilage ECM deposition, illustrating the enhanced chondrogenesis of ASCs was achieved. At the same time, osteogenic genes were also detected during 7 days induction, expression of which were none detectable, indicating the presence of

TGF-β1, IGF-1 and BMP-2 were cooperated to drive the chondrogenic differentiation of ASCs without activating osteogenesis. As known that BMP-2 alone appears to stimulate osteogenesis, while when used together with other growth factors such as IGF-1, BMP-2 is capable of stimulating chondrogenesis [13,38,39]. After 7 days, the scaffold carrying induced ASCs in both layers and residual BMP-2 mainly in subchondral layer was transplanted into osteochondral defects for *in vivo* generation. The complete *in vivo* regeneration of cartilage layer was only found in group I, indicating the importance of *in vitro* initiation of chondrogenesis.

During *in vivo* regeneration in the present study, BMP-2 played a critical role to accelerate subchondral bone regeneration, thus promoted the morphological and functional rebuilding of cartilage layer, limiting osteoarthritis development. The positive effect was confirmed by the histological examination results in group II compared with group III. In group II, after 12 weeks post-implantation, neo-bone tissues were observed in subchondral regions. However, few trabecular bone could be observed in group III without BMP-2. Without the support of neo-bone, the surrounding native bone collapsed as shown in **Fig. 7,8**. Accordingly, BMP-2 possesses the ability to enhance the recruitment of MSCs to cartilage condensations, to modulate expansion of condensation size, as well as to initiate BMP-dependent signaling cascades in mesenchymal progenitor cells for the induction of chondrogenesis and osteogenesis [40]. In group II without *in vitro* chondrogenic induced ASCs, BMP-2 was transplanted *in vivo* to induce autologous bone marrow derived mesenchymal stem cells (BMSCs) to undergo chondrogenesis and

osteogenesis in turn to generate bone tissue. As the *in vivo* results exhibited, cartilage specific ECM including GAGs and COL II were firstly observed at 6 weeks post-implantation, which were then disappeared and replaced by bone matrix when it came to 12 weeks. In addition, although subchondral bone defects were repaired by neo-bone tissue in group II, the morphology and bone specific ECM deposition were different from normal bone. However, group I carrying chondrogenic induced ASCs and BMP-2 exhibited significant regeneration of trabecular bone as early as 6 weeks, and the most complete bone regeneration at 12 weeks among the three groups, indicating initiation of chondrogenesis *in vitro* could also accelerate and enhance the *in vivo* bone regeneration. G. Zhou [41] showed a similar result that chondrogenic pre-induced BMSCs resulted in a better subchondral bone regeneration *in vivo*. And endochondral ossification may play an important role. As C. M. Shea [42] illustrated, BMP induced MSCs to undergo a sequential pattern of chondrogenic followed by osteogenic differentiation that was dependent on the continuous presence of BMP. In the present study, chondrogenesis was triggered *in vitro*, and the following endochondral ossification was achieved by the presence of BMP-2 carried by scaffold O, thus accelerating subchondral bone regeneration *in vivo*.

Finally, as the multi-tissues regeneration, one of the most important parameters was regeneration of the cartilage-bone interface. Osteochondral scaffolds were always expected to perform better on interface generation. In the present study, the regenerated cartilage-bone interface was also evaluated by histological examination and EDX. In regenerated region, the neo-cartilage in group I at 12 weeks possessed

zone of calcified cartilage, which connecting the neo-cartilage and neo-bone. EDX further confirmed the presence of continuous, gradual transition of Ca and P, indicating the existence of transition structure.

5. Conclusion

The present study offered an osteochondral scaffold, which was consisted of the PLGA/CS hydrogel and PLGA/CS/nHA-g-PLGA PEC to achieve distinguishing BMP-2 binding capability to induce hyaline-like cartilage and subchondral bone regeneration simultaneously. ASCs were aggregated spontaneously to form spheroids in-situ inside of chemical cross-linked PLGA/CS chondrogenic scaffold. The *in vitro* chondrogenesis of ASCs, as well as *in vivo* hyaline-like cartilage regeneration were thus enhanced. nHA-g-PLGA was synthesized to fabricate scaffold with better mechanical performance. Also, PLGA/CS/nHA-g-PLGA PEC bone scaffold possessed the ability to bind abundant BMP-2 for *in vivo* stimulating subchondral bone regeneration. The *in vivo* regeneration of cartilage was not only performed like normal hyaline cartilage, but also supported by the simultaneous regeneration of underlying bone.

Acknowledgements

The work was supported by the National Natural Science Foundation of China (Nos. 51173101, 51373094, 51503119), the Science and Technology Commission of Shanghai Municipality (No. 15JC1490400), China Postdoctoral Science Foundation (No. 2014M560324).

Author contributions

Kunxi Zhang carried out fabrication of scaffold and structural characterization, the cell culture, animal studies and tissue analyses. Shiming He and Guifei Li carried out the poly(L-glutamic acid) and nHA-g-PLGA synthesis. Danqing Zhang carried out fabrication of scaffold and structural characterization. Shifeng Yan contributed to assistance of data analysis. Jingbo Yin, Lei Cui were responsible for the overall project design and manuscript organization. Kunxi Zhang, Lei Cui and Jingbo Yin contributed to the scientific planning, data analysis and interpretation.

References

[1] Y. Wu, *et al*, *Adv. Funct. Mater.,* 2014, **24**, 4473.

[2] D. B. Burr and M. A. Gallant, *Nat. Rev. Rheumatol.,* 2012, **8**, 665.

[3] J. Chen, *et al*, *Biomaterials,* 2011, **32**, 4793.

[4] H. H. Yoon, *et al*, *Tissue Eng. A,* 2012, **18**, 1949.

[5] D. J. Huey, *et al*, *Science,* 2012, **338**, 917.

[6] K. Zhang, et al, *Biomaterials*, 2015, **71**, 24.

[7] A. K. Lynn, *et al*, *J. Biomed. Mater. Res. A,* 2010, **92**, 1057.

[8] W. Bonfield, *et al*, *Biomaterials,* 1981, **2***,* 185.

[9] E. Kon E, *et al*, *Injury,* 2010, **41***,* 693.

[10] T. J. Levingstone, *et al*, *Acta Biomater.,* 2014, **10***,* 1996.

[11] K. Zhang, *et al*, *Acta Biomater.,* 2013, **9**, 7276.

[12] N. Mohan, *et al*. *Tissue Eng. Part A,* 2011, **17**, 2845.

[13] M. Knippenberg, *et al*, *Biochem. Biophys. Res. Commun.,* 2006, **342***,* 902.

[14] X. Dong, *et al*, *Biophys. J.,* 2007, **93**, 750.

[15] T. A. Holland, *et al*, *J. Biomed. Mater. Res. A*, 2005, **75**, 156.

[16] G. Zhen, *et al*, *Nat. Med.,* 2013, **19**, 704.

[17] Q. Wang, *et al*, *Nat. Med.,* 2011, **17**, 1674.

[18] H. Madry, *et al*, *Knee Surg. Sports Traumatol. Arthrosc.,* 2010, **18**, 419.

[19] R. J. Lories and F. P. Luyten, *Nat. Rev. Rheumatol.,* 2011, **7**, 43.

[20] D. Nathan, *et al*, *Ann. Biomed. Eng.,* 2010, **38**, 2121.

[21] S. Alexander and J. M. McBirnie, *Shoulder and Elbow*, 2012, **4**, 179.

[22] P. E. Gelber, *et al*, *Knee*, 2014, **21**, 827.

[23] R. Thull, *Materialwiss. Werkst.,* 2001, **32**, 949.

[24] J. Fang, *et al*, *Acta Biomater.*, 2014, **1**, 276.

[25] S. Yan, *et al*, *J. Mater. Chem. B,* 2013, **1**, 1541.

[26] S. Nuernberger, *et al*, *Biomaterials,* 2011, **32**, 1032.

[27] S. H. Hsu and G. S. Huang, *Biomaterials,* 2013, **34**, 4725.

[28] T. J. Bartosh, *et al*, *Proc. Natl. Acad. Sci. USA,* 2010, **107**, 13724.

[29] L. Zhang, *et al*, *Biotechnol. Lett.,* 2010, **32**, 1339.

[30] J. E. Frith, *et al*, *Tissue Eng. Part C,* 2010, **16**, 735.

[31] Y. J. Yin, *et al*, *J. Appl. Polym. Sci.,* 2000, **77**, 2929.

[32] C. A. W. Andrew, *et al*, *J. Biomed. Mater. Res. A,* 1998, **41**, 541.

[33] W. Tachaboonyakiat, *et al*, *Polym. J.,* 2001, **33**, 177.

[34] X. Cai, *et al*, *Acta Biomater.,* 2009, **5**, 269.

[35] H. Zhou, *et al*, *Biochem. Biophys. Res. Commun.,* 2007, **361**, 91.

[36] H.W. Choi, *et al*, *J. Colloid Interface Sci.,* 2006, **304**, 277.

[37] A. Wörz, *et al*, *J. Mater. Chem.,* 2012, **22**, 19547.

[38] C. An, *et al*, *Ann. Biomed. Eng.,* 2010, **38**, 1647.

[39] B. Schmitt, *et al*, *Differentiation,* 2003, **71**, 567.

[40] B.K. Hall and T. Miyake, *Bioessays,* 2000, **22**, 138.

[41] G. Zhou, *et al*, *Tissue Eng.*, 2006, **12**, 3209.

[42] C. M. Shea, *et al*, *J. Cell Biochem.*, 2003, **90**, 1112.

Figure legends

Fig. 1. The schematic of the osteochondral scaffold design strategy.

Fig. 2. Synthesis of nHA-g-PLGA. a, nHA-g-PLGA was synthesized by initiating NCA polymerization in the surface of nHA-NH_2 particle which was amino-functionalized from nHA, followed by removing the benzyl-protecting groups with Me_3SiI. b, TEM images of nHA and nHA-g-PLGA. c, XPS survey scan of nHA and nHA-g-PLGA. d, XPS C 1s spectra of nHA and nHA-g-PLGA. The C 1s spectral envelopes were deconvoluted in a C-C, C-H peak at 285.0 eV, a C-N peak at 286.0 eV, a N-C=O peak at 288.2 eV, and a O-C=O peak at 289.0 eV. e, FT-IR spectra. f, TGA for nHA cores and nHA-g-PLGA nanoparticles produced at 0.08, 0.16, 0.32 mol/L of [M]. g, The measured and estimated Gr of nHA-g-PLGA.

Fig. 3. Evaluation of osteogenic scaffold (scaffold O) fabricated by nHA-g-PLGA. Scaffold fabricated by nHA was employed as control group. a, Monitoring of time-dependent colloidal stability of nHA, PLGA and nHA-g-PLGA. b, SEM image of scaffold fabricated by nHA-g-PLGA. c, SEM image of scaffold fabricated by nHA. d and e were higher-magnification images selected from b and c, respectively. f, g, h and i were EDS spectra of the inner walls of pores. j, storage modulus of scaffolds fabricated by adding different amount of nHA and nHA-g-PLGA, illustrating the improvement of mechanical property could be achieved when nHA-g-PLGA was involved in scaffold construction.(Bar scales: 100 μm for b & c, 50 μm for d & e. $*P < 0.05$, # and @ mean the data was significantly different to the others).

Fig. 4. Evaluation of chemical cross-linking process. a, NHS and EDC were employed to activate the γ-carboxyl of PLGA, followed by reacting with the amino groups of CS. b, Gelation time point detected by dynamic mechanical test. c, 50, 60 and 70 s were chose to carry out the combination of scaffold O and scaffold C, shear strength was evaluated to choose the optimize time point for osteochondral scaffold constructing. *$P < 0.05$.

Fig. 5. Evaluation of osteochondral scaffold. a, Gross appearance and inner structure of osteochondral scaffold, as well as Ca and P distribution at osteochondral scaffold interface. b, Pore structure of scaffold C. c, Pore structure of scaffold O. d, Pore size of scaffold C and scaffold O. e, Porosity of scaffold C, scaffold O and scaffold OC. f, Swelling ratio. g, compressive moduli. h, Shear deformation curve at the interface of integrated scaffold OC. i, Surface zeta potentential of scaffold C and scaffold O. j, BMP-2 association of scaffold C and scaffold O. k, BMP-2 association scaffold C and scaffold O after releasing *in vitro* for 3, 7 and 14 days. (Bar scales: 300 μm for a, 100 μm for b & c. *$P < 0.05$).

Fig. 6. Distribution, proliferation and differentiation of ASCs in osteochondral scaffold. a and c, Dio pre-labeled ASCs distribution in scaffold C and scaffold O at 4 h post-seeding, respectively. b, At 72 h post-seeding, ASCs aggregated to form spheroids in scaffold C. d, The adherent ASCs in scaffold O exhibited significant proliferation, as observed through the more extensive green fluorescence. e, Merged images to show ASCs distribution in the osteochondral scaffold. f and g, images of ASC spheroids and adherent ASCs in scaffold C and scaffold O, respectively. h and i,

DNA content in scaffold C and scaffold O, respectively. The proliferation of ASCs in scaffold C was limited. j, Quantitation of amounts of deposited COL II, COL I and GAGs after *in vitro* chondrogenic induction for 7 days. k, Relative ratio of cartilage genes expression in scaffold C and scaffold O. The gene expression levels are normalized to that of GAPDH. The relative gene expression of the non-induced group in day 0 was set as 1. (Bar scales: 100 μm for all. $*P < 0.05$).

Fig. 7. Morphological evaluation of neo-tissue in critical-size rabbit osteochondral defects. Group I: scaffold with induced ASC spheroids and BMP-2; group II: bare scaffold with BMP-2; group III: bare scaffold. (Bar scales: 1000 μm for a1,b1,c1,d1,e1,f1, 100 μm for a2,b2,c2,d2,e2,f2).

Fig. 8. Evaluation of cartilage ECM and bone ECM deposition through Safranin O & fast green staining, COL II immunohistochemical staining images and COL I immunohistochemical staining in group I ,II and III at 6 w and 12 w, respectively. (Bar scales: 1000 μm for all).

Fig. 9. The worst repaired defect of each group at 12 weeks (a). Biochemical evaluation, biomechanical evaluation and evaluation of osteochondral tissue interface. b, GAGs content. c, COL II content. d, Compressive moduli. e, Ca and P distribution at osteochondral tissue interface. (Bar scales: 1000 μm for all, 500 μm for the higher-magnification image selected from group I. $*P < 0.05$)

Figures

Fig. 1.

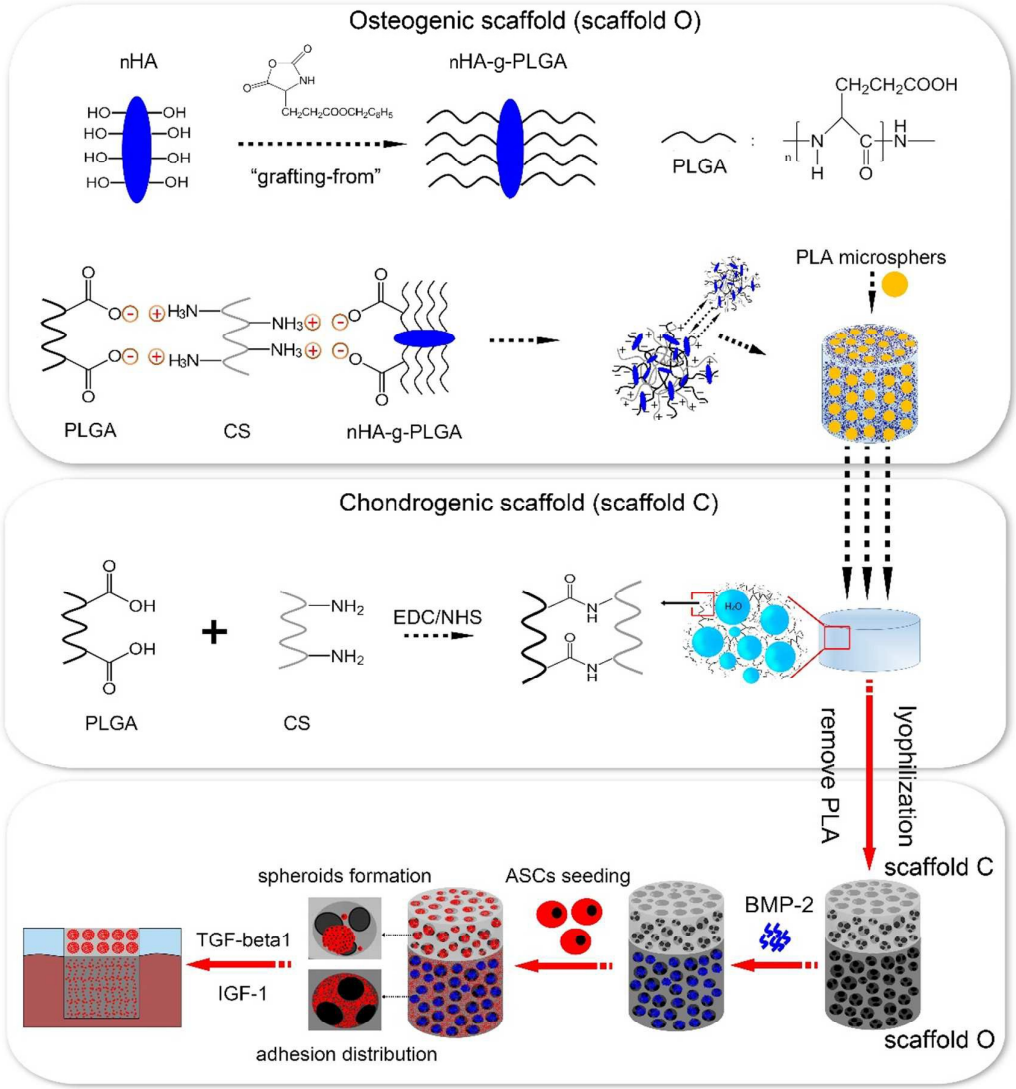

Fig. 2.

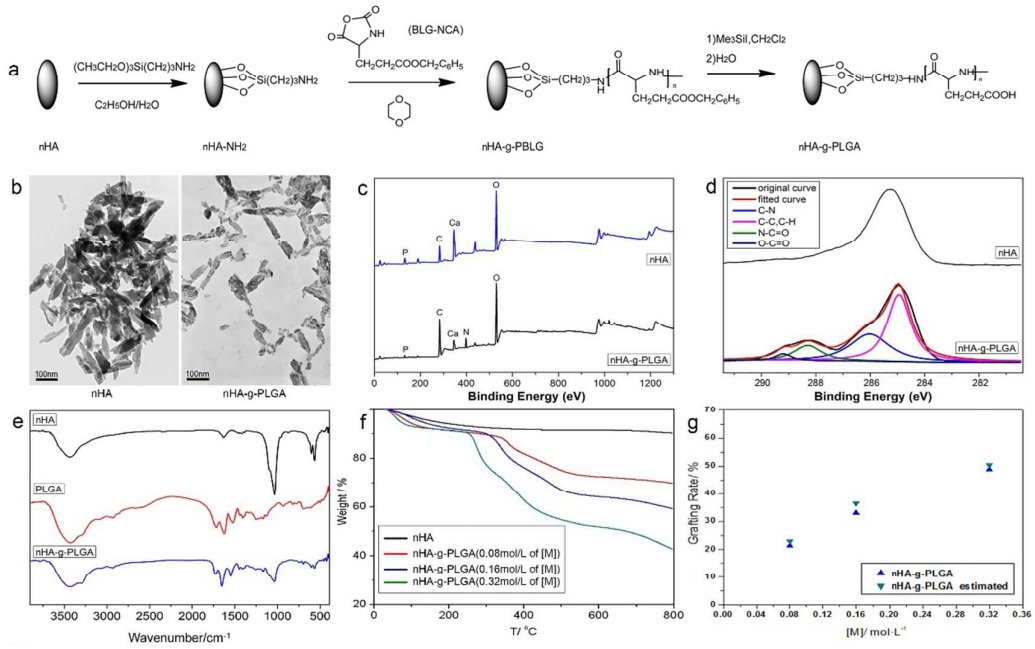

Fig. 3.

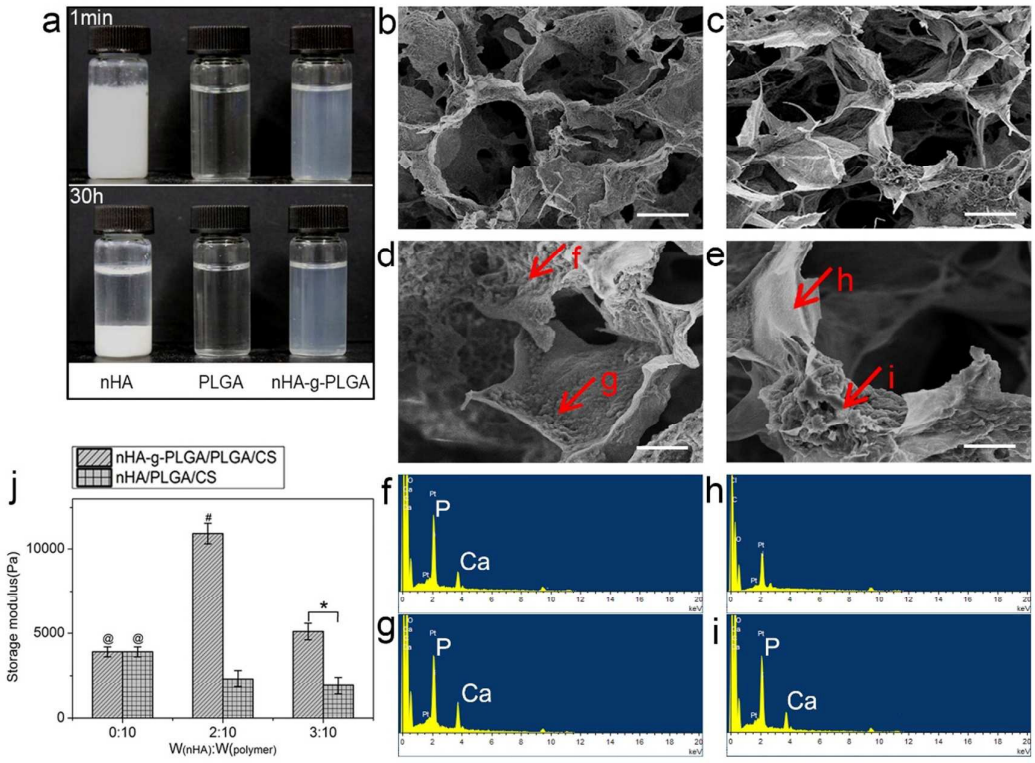

Fig. 4.

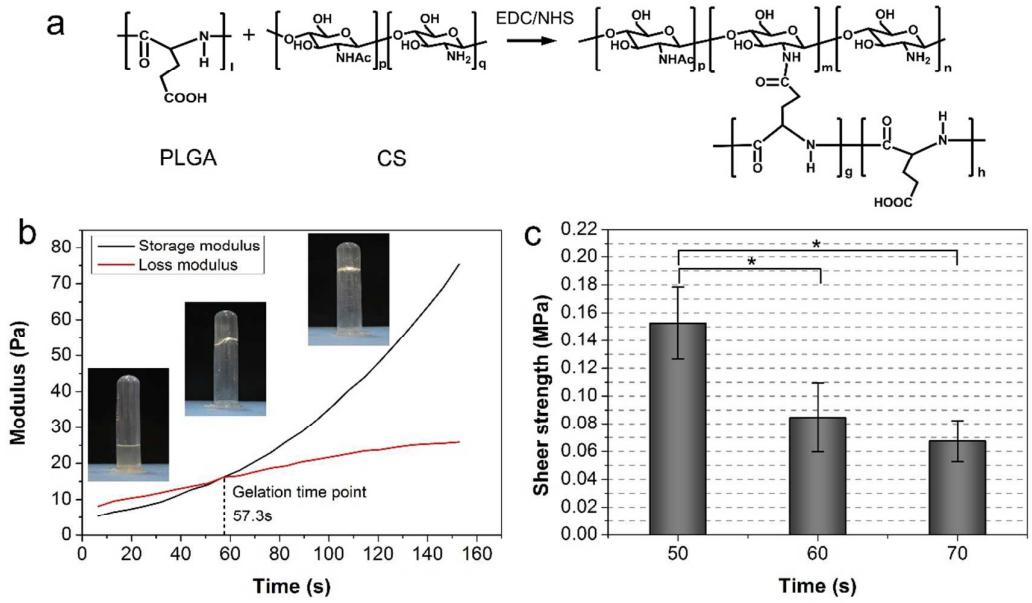

Fig. 5.

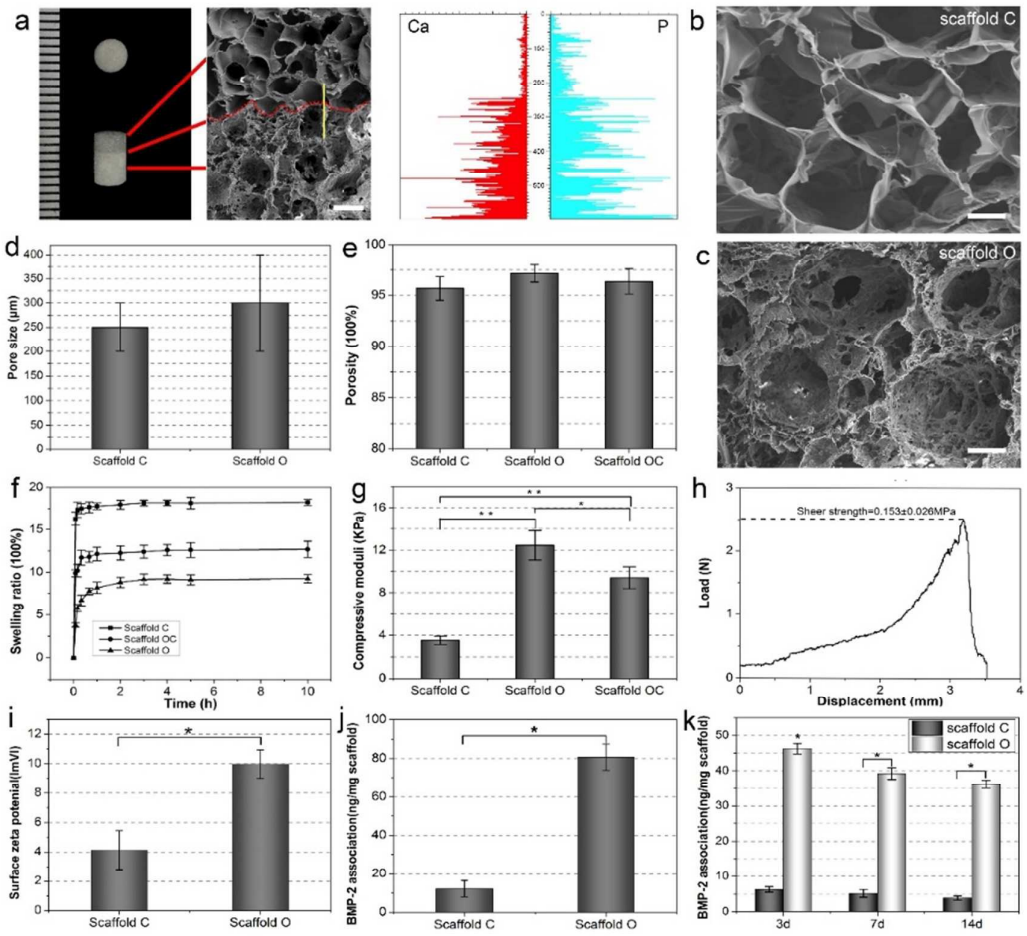

Fig. 6.

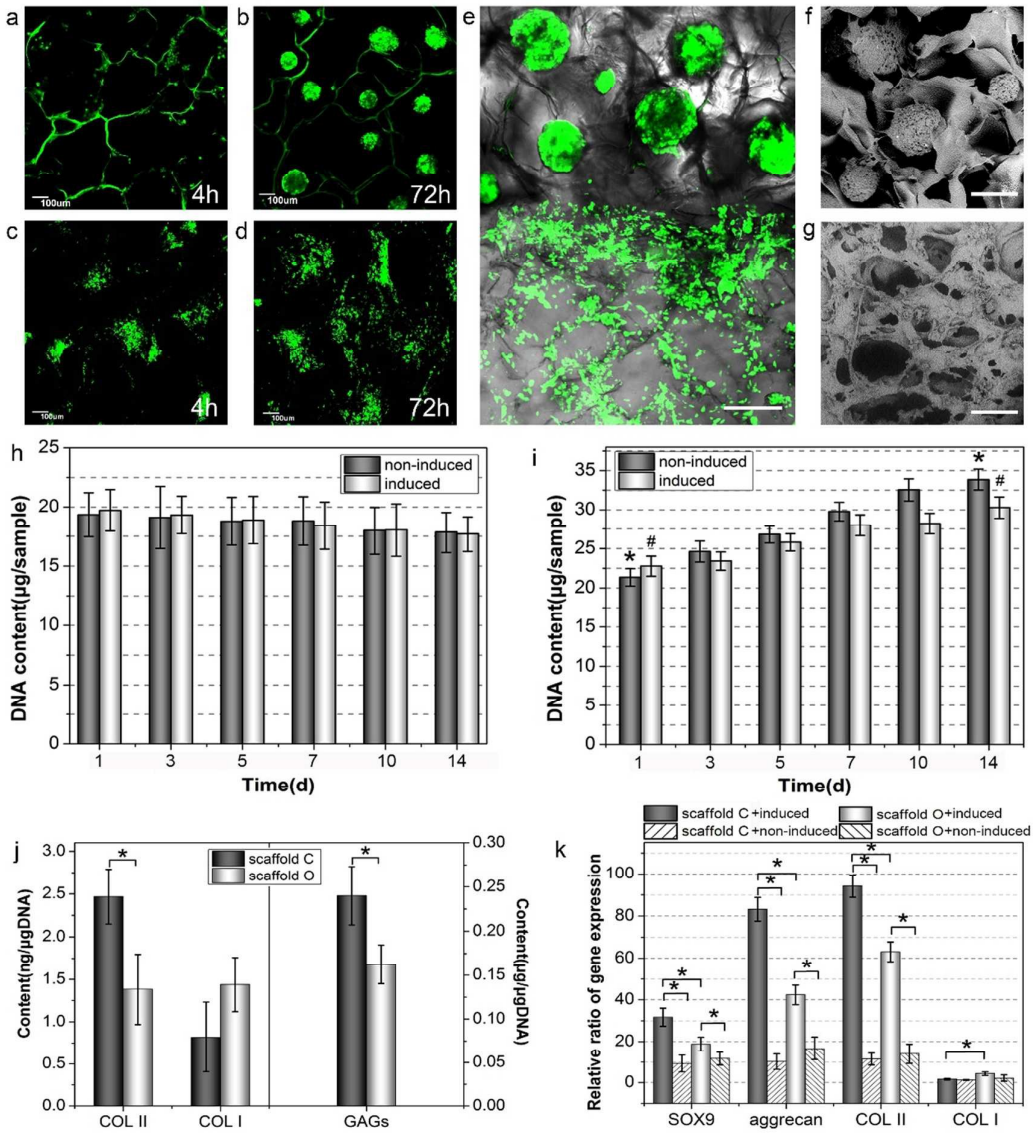

Fig. 7.

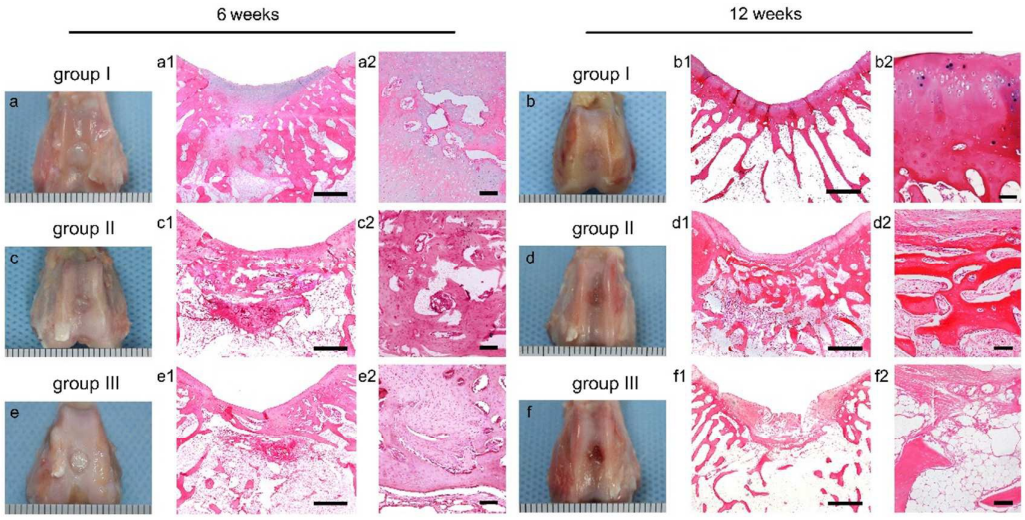

Fig. 8.

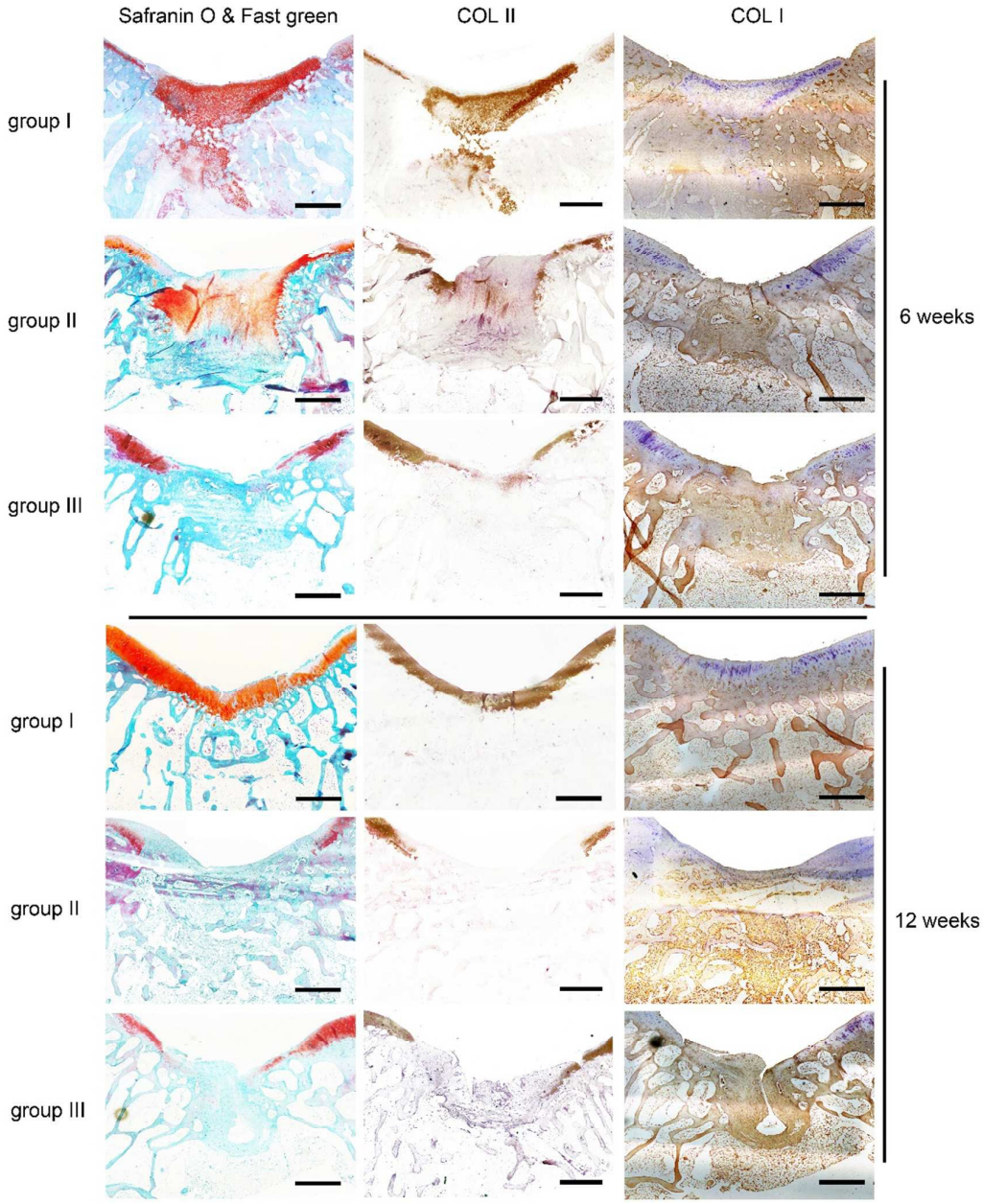

Fig. 9.

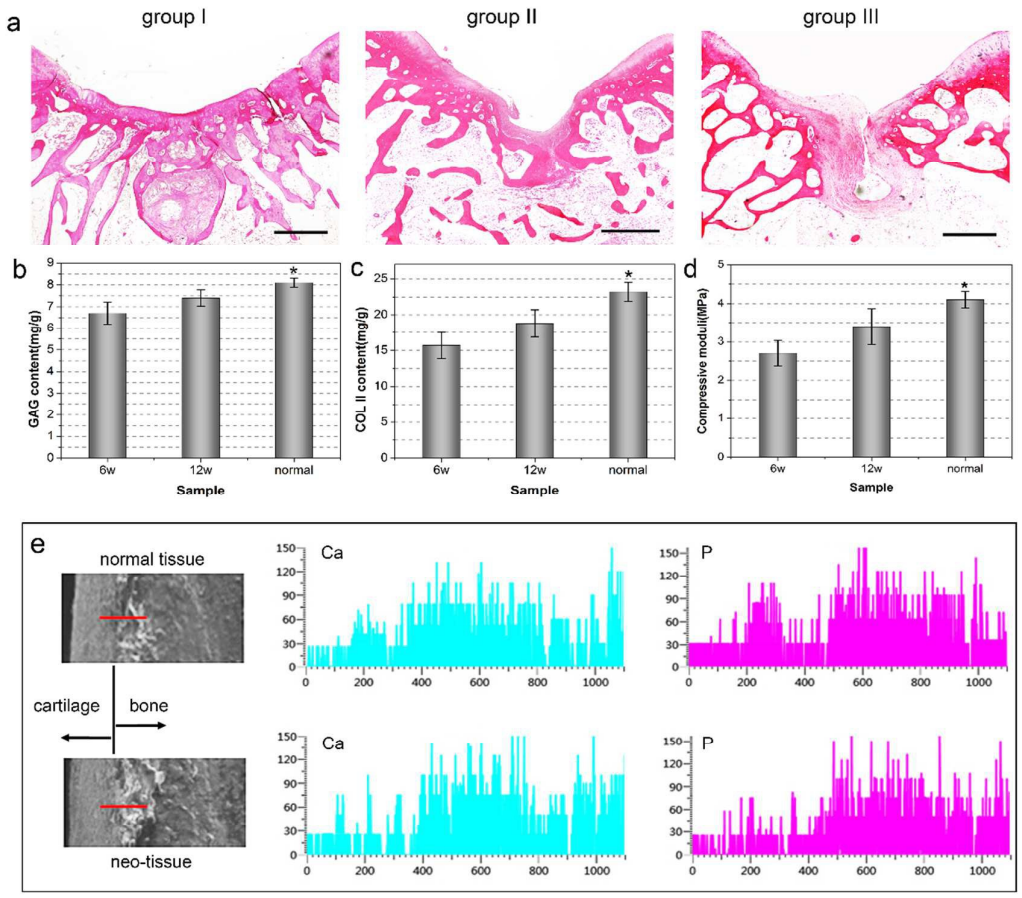

Tables

Table 1 Primer sequences.

gene	Primer sequences: rabbit,
GAPDH	5'-CCCTCAATGACCACTTTGTGAA-3' 5'-AGGCCATGTGGACCATGAG-3'
COL II	5'-ATGGACATTGGAGGGCCTGA-3' 5'-TGTTTGACACGGAGTAGCACCA-3'
COL I	5'-AAGGGTGAGACAGGCGAACAA-3' 5'-TTGCCAGGAGAACCAGCAAGA-3'
Aggrecan	5'-AGGTCGTGGTGAAAGGTGTTG-3' 5'-GTAGGTTCTCACGCCAGGGA-3'
SOX9	5'-GGTGCTCAAGGGCTACGACT-3' 5'-GGGTGGTCTTTCTTGTGCTG-3'
ALP	5'-CAGGATTGACCACGGGCACC-3' 5'-GCCTGGTAGTTGTTGTGAGC-3'
OCN	5'-ATGAGGACCCTCTCTCTGCT-3' 5'-GTTGAGCTCACACACCTCCC-3'

Table 2 Experimental groups carried out *in vivo*.

group I	Induced ASC spheroids in scaffold with BMP-2

group II	Bare scaffold with BMP-2
group III	Bare scaffold

Table 3 In vivo examination design.

	6 weeks			12 weeks		
Group	I	II	III	I	II	III
Total rabbit number	7	7	7	7	7	7
Total sample number	14	14	14	14	14	14
Rabbits used in histological examination	5	7	5	5	6	5
Samples used in histological examination	5	7	5	5	6	5
Sections per sample	4	4	4	4	4	4
Total section number	20	28	20	20	24	20

Table 4 Histological Scoring System for Evaluation of Overall Tissue Filling (a), Subchondral Bone Repair (b), and Cartilage Repair (c) in Rabbit, Osteochondral Defects [15].

(a) Overall defect evaluation (throughout the entire defect depth)	**Score**
1.Percent filling with neo-formed tissue	
100%	3
> 50%	2
< 50%	1
0%	0
2.Percent degradation of the implant	
100%	3

> 50%	2
< 50%	1
0%	0
(b) Subchondral bone evaluation (within the bottom 2 mm of defect)	
3. Percent filling with neo-formed tissue	
100%	3
> 50%	2
< 50%	1
0%	0
4. Subchondral bone morphology	
Normal, trabecular bone	4
Trabecular, with some compact bone	3
Compact bone	2
Compact bone and fibrous tissue	1
Only fibrous tissue or no tissue	0
5. Extent of neo-tissue bonding with adjacent bone	
Complete on both edges	3
Complete on one edges	2
Partial on both edges	1
Without continuity on either edge	0
(c) Cartilage evaluation (within the upper 1 mm of defect)	
6. Morphology of neo-formed surface tissue	
Exclusively articular cartilage	4
Mainly hyaline cartilage	3
Fibrocartilage	2
Only fibrous tissue or bone	1
No tissue	0
7. Thickness of neo-formed cartilage	
Greater than surrounding cartilage	3
Similar to the surrounding cartilage	2
Less than the surrounding cartilage	1
No cartilage	0
8. Joint surface regularity	
Smooth, intact surface	3
Surface fissures (< 25% neo-surface thickness)	2
Deep fissures (25-99% neo-surface thickness)	1
Complete dissruption of the neo-surface	0
9. Chondrocyte clustering	

None at all	3
< 25% chondrocytes	2
25-100% chondrocytes	1
No chondrocytes present (no cartilage)	0
10. Cell and glycoasminoglycan (GAG) content of neo-formed cartilage	
Normal cellularity with normal Safranin O staining	3
Normal cellularity with moderate Safranin O staining	2
Clearly less cells with poor Safranin O staining	1
Few cells with no or little Safranin O staining or no cartilage	0
11. Collagen content	
Normal	3
Moderately reduced	2
Severly reduced	1
Absent or no cartilage	0
12. Cell and glycoasminoglycan (GAG) content of adjacent cartilage	
Normal cellularity with normal GAG content	3
Normal cellularity with moderate GAG content	2
Clearly less cells with poor GAG content	1
Few cells with no or little GAGs or no cartilage	0

Table 5 Results of histological grading for osteochondral tissue regeneration.

Histological Parameter	**6 weeks**			**12 weeks**		
	group I	**group II**	**group III**	**group I**	**group II**	**group III**
Overall defect evaluation						
1. Percent filling with neo-formed tissue	2.7 ± 0.2^{b}	2.4 ± 0.4^{c}	$1.6\pm0.3^{b,c}$	$2.8\pm0.2^{b,c}$	$2.2\pm0.2^{b,c}$	$1.1\pm0.3^{b,c}$
2. Percent degradation of the implant	2.3 ± 0.2^{a}	2.2 ± 0.3^{a}	2.1 ± 0.2^{a}	2.9 ± 0.1^{a}	2.9 ± 0.1^{a}	2.8 ± 0.2^{a}
Subchondral bone evaluation						
3. Percent filling with neo-formed tissue	2.6 ± 0.3^{b}	2.7 ± 0.5^{c}	$1.4\pm0.4^{a,b,c}$	2.6 ± 0.5^{b}	2.7 ± 0.2^{c}	$0.3\pm0.1^{a,b,c}$
4. Subchondral bone morphology	$2.3\pm0.2^{a,b}$	$1.5\pm0.3^{a,b}$	0.6 ± 0.4^{b}	$3.1\pm0.5^{a,b}$	$2.0\pm0.2^{a,b}$	0.4 ± 0.2^{b}
5. Extent of neo-tissue bonding with adjacent bone	2.8 ± 0.2^{b}	1.9 ± 0.4^{b}	0.6 ± 0.2^{b}	2.9 ± 0.1^{b}	2.1 ± 0.4^{b}	0.3 ± 0.2^{b}
Cartilage evaluation						
6. Morphology of neo-formed surface tissue	$2.7\pm0.3^{a,b,c}$	$2.1\pm0.2^{a,b}$	$1.8\pm0.5^{a,c}$	$3.4\pm0.3^{a,b}$	$1.4\pm0.2^{a,b}$	$0.7\pm0.3^{a,b}$
7. Thickness of neo-formed cartilage	$2.9\pm0.1^{a,b}$	$2.1\pm0.3^{a,b}$	$0.9\pm0.4^{a,b}$	$2.2\pm0.3^{a,b,c}$	$0.3\pm0.3^{a,b}$	$0.2\pm0.2^{a,c}$
8. Joint surface regularity	$2.3\pm0.2^{a,b,c}$	$1.5\pm0.4^{a,b}$	$0.9\pm0.2^{a,c}$	$2.7\pm0.1^{a,b,c}$	$0.5\pm0.4^{a,b}$	$0.2\pm0.2^{a,c}$
9. Chondrocyte clustering	$1.7\pm0.4^{a,b}$	$1.0\pm0.2^{a,b}$	$0.4\pm0.3^{a,b}$	$2.5\pm0.1^{a,b,c}$	$0.3\pm0.3^{a,b}$	$0.0\pm0.0^{a,c}$

10. Cell and GAG content of neo-formed cartilage	2.8 ± 0.1^{b}	$1.7\pm0.4^{a,b}$	$0.7\pm0.3^{a,b}$	$2.8\pm0.1^{b,c}$	$0.2\pm0.1^{a,b}$	$0.2\pm0.1^{a,c}$
11. Collagen content	$2.8\pm0.1^{b,c}$	$1.5\pm0.5^{a,b}$	$0.8\pm0.3^{a,c}$	$2.8\pm0.1^{b,c}$	$0.2\pm0.1^{a,b}$	$0.2\pm0.2^{a,c}$
12. Cell and GAG content of adjacent cartilage	$2.9\pm0.1^{b,c}$	2.1 ± 0.2^{b}	2.0 ± 0.4^{c}	$2.9\pm0.1^{b,c}$	2.4 ± 0.4^{b}	1.8 ± 0.3^{c}

Values are shown as mean±standard deviation. [a] $p < 0.05$ vs. 6 week data. [b,c] $p < 0.05$ vs. the other group.